Available online at www.sciencedirect.com
SCIENCE DIRECT®
Journal of the European Ceramic Society 25 (2005) 927–933
www.elsevier.com/locate/jeurceramsoc

Mechanical properties of $LaFeO_3$ ceramics

A. Fossdal, M.-A. Einarsrud, T. Grande*

Department of Materials Technology, Norwegian University of Science and Technology, Sem Sælands vei 12, N-7491 Trondheim, Norway

Received 28 January 2004; received in revised form 27 March 2004; accepted 25 April 2004
Available online 3 July 2004

Abstract

The fracture strength, fracture toughness and apparent Young's modulus of $LaFeO_3$ ceramics in the temperature region 25–800 °C are reported. The fracture strength of the material was observed to increase from 202 ± 18 MPa at room temperature to 235 ± 38 MPa at 800 °C. The room temperature fracture toughness was 2.5 ± 0.1 MPa $m^{1/2}$. The fracture toughness decreased to 2.1 ± 0.1 MPa $m^{1/2}$ at 600 °C, followed by an increase to 3.1 ± 0.3 MPa $m^{1/2}$ at 800 °C. The temperature dependence of the fracture toughness correlates well with the crystallographic strain, $|(a-c)|/(a+c)$, and ferroelastic toughening of $LaFeO_3$ materials is inferred. Non-elastic stress–strain behaviour of the $LaFeO_3$ materials due to ferroelasticity was confirmed by cyclic compression experiments, and residual strain was observed in the material after unloading.

Keywords: $LaFeO_3$; Mechanical properties; Strength; Toughness

1. Introduction

$LaFeO_3$ has an orthorhombic crystal structure with only three valent iron and is an antiferromagnetic insulator at room temperature.[1,2] Substitution of Sr for La increases the electronic and oxygen ionic conductivity and $La_{1-x}Sr_xFeO_{3-\delta}$ materials thus have potential applications as gas sensors, oxygen permeable membranes, electrodes in solid oxide fuel cells and oxidation catalysts.[3–11] In such high-temperature electrochemical devices, the mechanical properties of the ceramic components are particularly important for estimating reliability. Among the mechanical properties of interest are fracture strength, Young's modulus, creep resistance and fracture toughness. Differences in thermal expansion coefficients of the constituent materials or chemical expansion of materials in an oxygen potential gradient introduce compressive or tensile stresses that can potentially lead to failure of the device.[12–14]

So far only limited information is available on the temperature dependency of the mechanical properties of perovskite materials. Typical values for the room temperature four-point bending strength of orthorhombic perovskites lie in the range 100–140 MPa,[15,16] whereas the fracture toughness, K_{IC}, is generally in the range 2.0–2.8 MPa $m^{1/2}$.[15,17] The bend strength and fracture toughness of orthorhombic perovskites tends to be constant or increase with temperature, followed by a decrease above the orthorhombic to rhombohedral phase transition temperature.[15–19] The room temperature four-point bending strength of rhombohedral and cubic perovskites has been reported in the range 100–160 MPa.[20,22] The strength of rhombohedral and cubic perovskites generally decreases with increasing temperature,[15,22,23] but the opposite behaviour has also been observed.[24] The fracture toughness of cubic and rhombohedral perovskites tends to be lower (K_{IC} = 1.3–2.2 MPa $m^{1/2}$ at room temperature)[21,25] than for orthorhombic materials and generally decreases or remains approximately constant with increasing temperature.[15,17,25]

Monolithic ceramics are usually brittle and show elastic behaviour when stress is applied. Some ceramics show non-elastic behaviour and have been termed ferroelastic by analogy with the stress–strain relationship with polarization of a ferroelectric material in an electric field and the magnetization of a ferromagnetic material in magnetic fields.[26] Ferroelastic behaviour has been observed in both rhombohedral and orthorhombic perovskites.[22,25,27–30]. Single crystal orthorhombic $LaFeO_3$ is ferroelastic at room temperature.[27] The crystal structure transforms to rhombohedral perovskite above 960–1005 °C.[31–33] Ferroelastic

* Corresponding author. Tel.: +47 73 59 40 84.
E-mail address: tor.grande@material.ntnu.no (T. Grande).

0955-2219/$ – see front matter © 2004 Elsevier Ltd. All rights reserved.
doi:10.1016/j.jeurceramsoc.2004.04.009

behaviour is also expected above the orthorhombic to rhombohedral phase transition by analogy with other rhombohedral perovskites. In this context it is important to note that the crystallographic origin of the ferroelasticity in the materials mentioned above is fundamentally different from well known ferroelastic behaviour of tetragonal PZT materials, which are also ferroelectric.[34]

The aim of this work was to obtain information on the mechanical properties of the $LaFeO_3$ as a function of temperature, and to relate these properties to structural properties. Finally, the mechanical properties are discussed with respect to ferroelasticity.

2. Experimental procedure

2.1. Sample preparation

$LaFeO_3$ powder was prepared by spray drying of a glycine/nitrate (G/N) solution. Approximately 1 M solutions of the metal nitrates were used. Glycine (Merck, ≥99.7%) was added at a molar ratio of 5/9[32] to that of the nitrates (all Merck, ≥99.0%), and the solution was then dried in a spray drier (Mini Spray-Drier B-191, BÜCHI) with an input temperature of 150 °C and a pump rate of 2 ml/min. The resulting powder was ignited by allowing it to fall through a vertical alumina tube heated to approximately 800 °C. The powders were ball milled overnight with Si_3N_4 balls and calcined in air for 24 h at 900 °C. The calcined powder was further ball milled overnight. The calcined powders were compacted into bars or cylinders by uniaxial double-action pressing at 20 MPa, followed by cold isostatic pressing at 200 MPa. The relative green density obtained was 50–58%. All powder compacts were sintered for 2 h at 1300 °C with a heating rate of 200 °C/h and a cooling rate of 100 °C/h. The density after sintering was 95–96% of theoretical.

2.2. Characterization

Polished (1 μm diamond finish) and thermally etched (0.1 h, 1200 °C) cross sections of selected sintered materials were investigated with a Hitachi S3500N scanning electron microscope (SEM). The mean grain size was estimated by averaging the maximum two-dimensional diameter of 225 grains. The microstructure was also investigated by transmission electron microscopy (TEM, Philips CM30, 300 kV).

X-ray powder diffraction (XRD) of calcined powders and sintered materials was performed on a Siemens D5005 θ–θ diffractometer using Cu Kα radiation and a secondary monochromator or a Siemens D5005 θ–2θ diffractometer using Cu Kα radiation and a primary monochromator.

Four-point bending strength and apparent Young's modulus (E-modulus) of machined specimens (Mil. Spec. 1942) were measured at ambient temperature and at 800 °C using a fully articulating 40/20 span SiC bend fixture (MTS Model 642.85) and a heating rate of 200 °C/h. Specimen dimensions were approximately 3 mm × 4 mm × 45 mm and 10 bars were tested at each temperature. All fracture surfaces were examined by SEM (Hitatchi S3500N) to reveal the fracture origin. Deflection of the specimen during loading was measured with a MTS Model 632.70–03 Bend Bar Extensometer with three pushrods (Model 602.81). The two outer pushrods were spaced to correspond with the location of the upper two rollers of the bend fixture. The deflection of the specimen was measured as the deflection of the centre pushrod with respect to the outer rods. The fracture toughness (K_{IC}) was determined in air at ambient, 400, 600 and 800 °C by the single edge notched beam (SENB) method and using the same bend fixture as above. The test bar dimensions were 3 mm × 4 mm × 45 mm, all machined to Mil. Spec. 1942. The test bar dimensions were not corrected for thermal expansion. The depth of the notches was 0.8 mm or 1.2 mm and the width was 0.2 mm. The fracture toughness was calculated using equations from ISO 15732.[35] A total of 3–4 bars were tested for each temperature. Testing was performed using a Cormet 20 kN electromechanical machine with a 2 kN HBM load cell and a Sigmatest controlled-atmosphere furnace with a Kanthal A element and nickel radiation shields. Before the high-temperature measurements, the sample chamber was evacuated and back-filled with synthetic air. The high-temperature measurements were performed in a flowing synthetic air atmosphere. All measurements were performed in position control, with a crosshead rate of 8 μm/s for four-point bend strength and 1 μm/s for SENB measurements.

Cyclic stress–strain relationship under compression was measured on a cylindrical sintered $LaFeO_3$ ceramic of diameter 4.1 mm and height 9.0 mm. The end surfaces of the cylinder were polished to a 1 μm diamond finish prior to testing, with a deviation in parallelism of less than 10 μm. The cylinder was placed between hardened steel compression plates and a preload of 20 MPa was applied. Subsequent loading and unloading of the test piece (down to 20 MPa) was performed, increasing the maximum load from 100 to 500 MPa in steps of 100 MPa. Compression was performed with a Dartec 20 kN servohydraulic universal testing machine with a 20 kN load cell. The load cell and actuator were mounted in a 250 kN Dartec frame. The strain was measured with an Instron ±1 μm two-sided averaging extensometer with 10 mm span, which was placed on the steel compression plates. Correction for fixture stiffness was performed by measuring the strain of an Al_2O_3 cylinder (same dimensions as the $LaFeO_3$ test cylinder) with well-known Young's modulus.[36] The measured strain of Al_2O_3 was compared with the theoretical linear strain, allowing determination of a correction function to be used on the $LaFeO_3$ raw data. The measurements were performed in load control, with a loading rate of 2 kN/min.

3. Results

3.1. Phase composition and micro structure

Analysis of X-ray diffractograms of calcined powder and of sintered materials both before and after mechanical testing showed single-phase orthorhombic $LaFeO_3$. The FWHM of the (1 2 1) reflection increased from 0.11° in powder samples to 0.14 and 0.23° in polished and machined ceramics, respectively. The line broadening of the machined samples was asymmetric.

SEM investigations confirmed the absence of secondary phases. Thermal etching at 1200 °C allowed for visual inspection of grain boundaries and the domain structure at the etching temperature. A micrograph of a polished and thermally etched specimen is shown in Fig. 1. The average grain size of the sintered materials was 3.3 ± 1.5 μm and the pores were sub-micron in size. The etching temperature is above the orthorhombic to rhombohedral phase transition of $LaFeO_3$, hence the lamellar domain structure observed within each grain represents that of the rhombohedral phase. A similar domain structure is also observed in other rhombohedral perovskites.[37,38]

The maximum number of twin boundaries observed by TEM in orthorhombic $LaFeO_3$ grains was three. About 50% of the investigated $LaFeO_3$ grains contained twin domains, the number increasing slightly after application of a mechanical stress of 500 MPa. Both straight and curved twin boundaries were observed. The twinning system is most likely identical to that observed for orthorhombic $La_{1-x}Sr_xMnO_3$ materials.[29]

3.2. Mechanical properties

The fracture strength of $LaFeO_3$ increased slightly with temperature, from 202 ± 18 MPa at room temperature to 235 ± 38 MPa at 800 °C. The scatter in fracture strength of the different test bars increased with increasing temperature, as shown in Fig. 2. The Weibull modulus was 10.5 and 5.8 at room temperature ($R^2 = 0.87$) and 800 °C ($R^2 = 0.81$), respectively. The fracture origins at both temperatures were porous regions with extension 50–100 μm, as seen from selected fractographs in Fig. 3. The fracture surface shows a transgranular fracture mode at both room temperature and

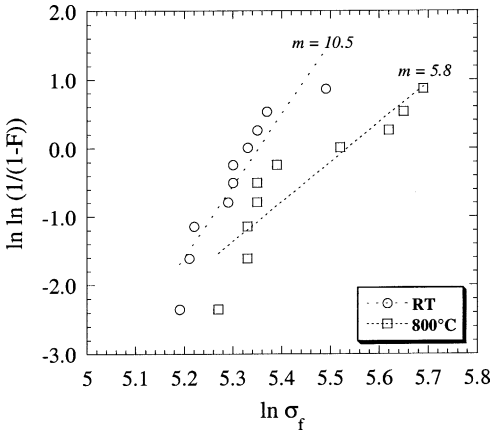

Fig. 2. Weibull analysis on the fracture strength values for $LaFeO_3$ tested at room temperature ($R^2 = 0.87$) and 800 °C ($R^2 = 0.81$).

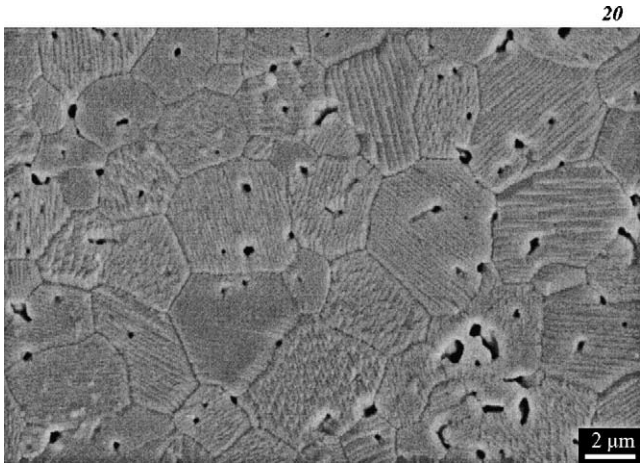

Fig. 1. SEM image of a polished and thermally etched section of $LaFeO_3$ sintered for 2 h at 1300 °C.

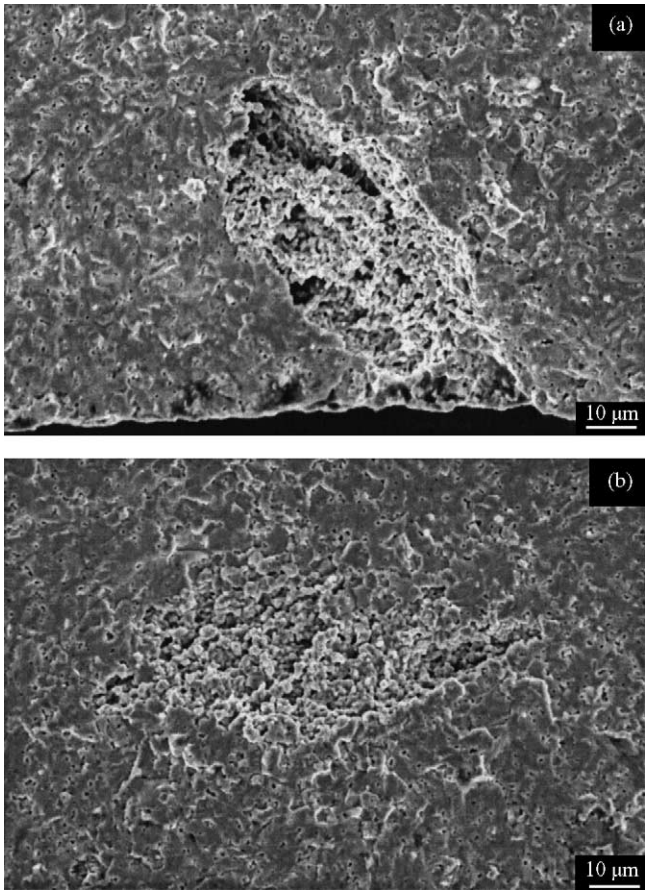

Fig. 3. Examples of fracture origins in the fracture strength measurements: (a) porous region close to the surface, (b) internal porous region.

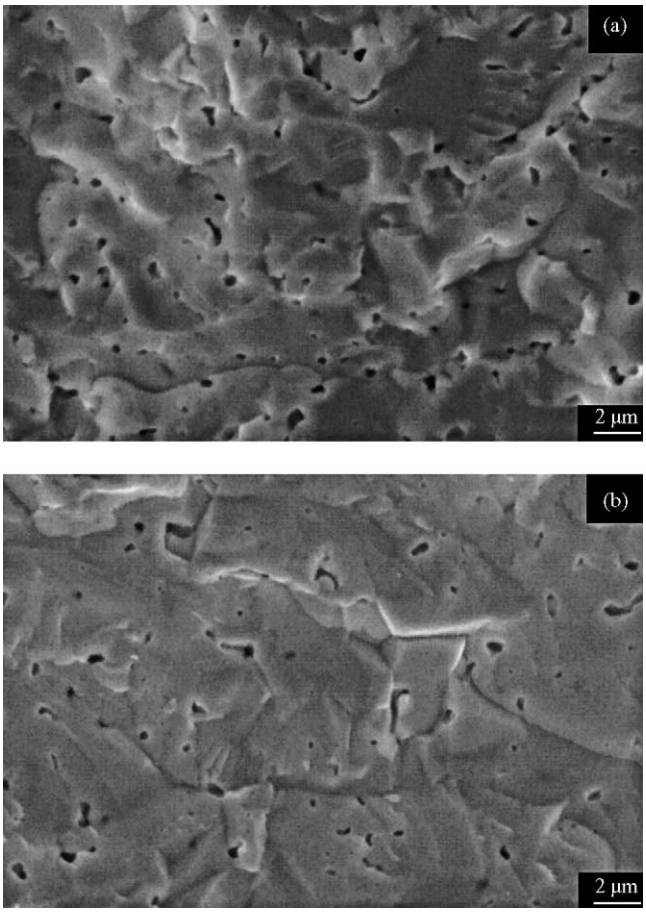

Fig. 4. SEM images showing transgranular fracture surfaces of bars tested at: (a) room temperature or (b) 800 °C.

800 °C (Fig. 4). No qualitative explanation for the lower Weibull modulus at 800 °C was found.

The stress–strain relationship under four-point bending was close to linear, but some minor deviation from linearity was observed at low load. Due to the non-linearity the apparent Young's modulus decreased with increasing applied stress. Extrapolation to zero applied stress gave a Young's modulus of 213 ± 14 GPa and 206 ± 24 GPa at room temperature and 800 °C, respectively. The non-linear stress–strain relationship gives a non-symmetric deformation behaviour and thereby a systematic overestimation of the strength.[39,40] The deviation from linear behaviour (see also Fig. 6) of the present materials is, however, small and the effect on the reported Young's modulus and bending strength is neglected.

The fracture toughness is given as a function of temperature and notch length in Fig. 5 along with the crystallographic strain, $|(a-c)|/(a+c)$, as defined by Abrahams et al.[27] The crystallographic strain is calculated from the cell parameters reported by Fossdal et al.[31] for $LaFeO_3$ as a function of temperature. The dashed line in Fig. 5 represents the crystallographic strain obtained from linear fits to the temperature-dependent cell parameters, whereas the measured values are shown as points. At 450–500 °C, the *a* and *c* axes cross, and by definition, $|(a-c)|/(a+c)$ is zero at this temperature. For a notch depth of 1.2 mm, the measured fracture toughness decreases slowly from 2.5 MPa $m^{1/2}$ at room temperature to 2.1 MPa $m^{1/2}$ at 600 °C. Above 600 °C, the fracture toughness increases steeply to 3.1 MPa $m^{1/2}$ at 800 °C. For a notch depth of 0.8 mm, the measured fracture toughness is 2.2 ± 0.1 MPa $m^{1/2}$ at room temperature and 2.7 MPa $m^{1/2}$ at 800 °C. Due to experimental difficulties, only a single bar was tested at 1000 °C (notch 0.8 mm), giving a fracture toughness of 3.1 MPa $m^{1/2}$.

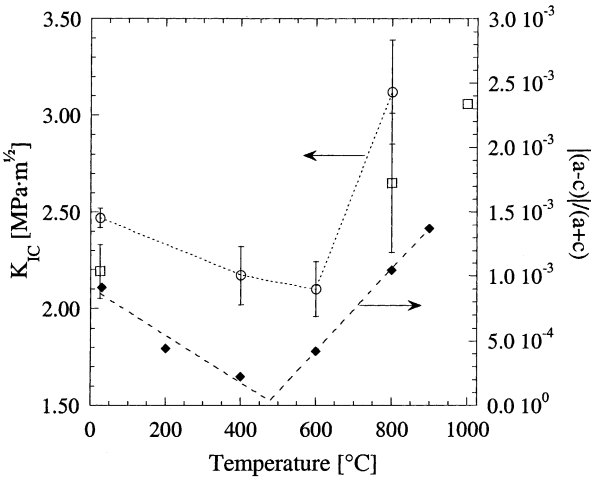

Fig. 5. Fracture toughness of $LaFeO_3$ as a function of temperature, measured by the SENB method with 1.2 mm notch (circles) and 0.8 mm notch (squares). The dotted line is a guide to the eye. Filled diamonds represent the crystallographic strain, $|(a-c)|/(a+c)$, calculated from Fossdal et al.[31] The dashed line is obtained from linear fits to the temperature dependent cell parameters.[31]

The temperature dependence of the fracture toughness and the correlation with crystallographic strain motivated a study of the strain-stress relationship under compression. The behaviour of $LaFeO_3$ under cyclic application and release of a pure compressive stress at room temperature is shown in Fig. 6. Non-elastic behaviour was observed in the

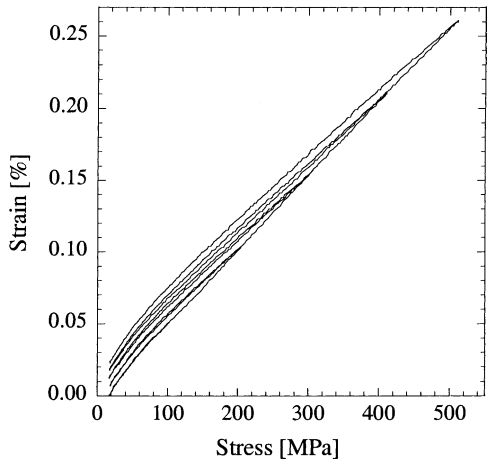

Fig. 6. Stress–strain behaviour during compressive cycling of a $LaFeO_3$ cylinder to progressively higher loads.

entire stress range of 20–500 MPa. The material shows a memory effect, as application of a load equal to the maximum load of the previous compressive cycle results in the same strain. The strain was fully relaxed after the first loading cycle, with a maximum stress of 100 MPa. Maximum stresses above 100 MPa gave a linear increase in the permanent strain with slope $5.95 \times 10^{-5}\%\,\mathrm{MPa}^{-1}$. The average apparent Young's modulus for stresses above 100 MPa was 195 ± 5 GPa, which is within the uncertainty of the modulus determined by the four-point bending tests.

4. Discussion

4.1. Compressive cycling behaviour

A ferroelastic material can be characterized by an elastic hysteresis in the stress–strain relation and by the presence of permanent strain in the material after unloading.[34] In order to obtain the complete ferroelastic hysteresis loop, the material has to be subjected to pure compressive stresses followed by pure tensile stresses. Only a part of the hysteresis loop for $LaFeO_3$ is shown in Fig. 6. We propose that the permanent strain in the partial hysteresis loop is due to switching of ferroelastic domains although we cannot rule out the possibility that microcracking may contribute to the total permanent strain at high loads. TEM gave, however, no indications of microcracking. No crystallographic evidence was found of a transformation from orthorhombic to rhombohedral crystal structure upon loading. A low coercive stress is expected from the narrow hysteresis loop, by analogy with soft magnets, suggesting that $LaFeO_3$ can be termed a soft ferroelastic material. The correlation between toughness and structural properties shown in Fig. 5 does give additional support this hypothesis, since reorientation of the domains must occur below the fracture stress in order to toughen the material. The coercive stress, σ_c, can be defined as the stress corresponding to the maximum in the effective compliance, s_{33}, defined as the derivative of the strain with respect to the stress.[41] By this approach, the coercive stress of $LaFeO_3$ is estimated to be in the order of 20 MPa. The lower value of σ_c for $LaFeO_3$ relative to $LaCoO_3$ (55 MPa) corresponds well with the wider hysteresis loop of the cobaltite.[42] The low coercive stress infers that the zero point of the strain, set at the preload of 20 MPa, is incorrect and that the curve in Fig. 6 should be slightly shifted towards higher strain.

Cycling the materials to increasingly higher compression load resulted in a linear increase in the permanent strain. This is not consistent with a soft ferroelastic behaviour and a coercive stress in the order of 20 MPa. Müllner and Kriven[43] proposed that nucleation of new twin boundaries in ferroelastic materials could occur at stresses significantly above σ_c. The observed permanent strain in $LaFeO_3$ ceramics at compressive stress levels above 100 MPa can be due to the generation of new deformation twins, but we cannot rule out microcracking as an alternative explanation. A third but less probable explanation of the increasing permanent strain with increasing maximum load is that $LaFeO_3$ is rather a hard ferroelastic material with coercive stress significantly above 0.5 GPa, the maximum load in our experiments. Further compression and possibly tension experiments are necessary in order to elucidate the soft–hard characteristics of ferroelastic $LaFeO_3$.

4.2. Fracture toughness

The stress–strain hysteresis loop provides a natural mechanism for dissipation of mechanical energy, and thus a mechanism for toughening.[44] As domains are switched, more work must be put in to advance the crack than would have been necessary in the absence of ferroelasticity, resulting in increased fracture toughness. The ferroelastic domains in the present material has a different structural origin compared to tetragonal PZT perovskite materials.[34,44] In PZT materials the domains are ferroelectric, and this is not the case for $LaFeO_3$. In PZT the ferroelasticity is caused by deformation of ZrO_6/TiO_6 octahedra, while in $LaFeO_3$ the octahedra are close to ideal. Twisting/bending of the octahedra causes the bonding angle between the octahedra to deviate from 180°, which corresponds to the bond angle in the cubic paraelastic state.

As a first approximation the contribution of ferroelasticity to fracture toughness can be approximated from[45]

$$K_{IC} \approx \frac{K_{IC}^{o}}{\sqrt{1 - 0.16\varepsilon_s E/\sigma_c}} \quad (1)$$

where K_{IC}^{o} denotes toughness in the absence of domain switching, σ_c is the coercive stress and ε_s is the switching strain of the polycrystalline material, which is proportional to the crystallographic strain, $|(a-c)|/(a+c)$. An increase in the crystallographic strain, other factors remaining constant, should thus increase the fracture toughness. This behaviour, and the corresponding decrease in fracture toughness with decreasing crystallographic strain, is seen for $LaFeO_3$.

$LaFeO_3$ ceramics are rhombohedral at 1000 °C.[31] The single SENB specimen measured at this temperature is insufficient to determine the fracture toughness accurately. Using the maximum of the measured uncertainties at the other temperatures, a lower estimate of the fracture toughness at 1000 °C is 2.7 MPa $m^{1/2}$. As rhombohedral $LaFeO_3$ is expected to be ferroelastic, also confirmed by the domain formation observed in Fig. 1, ferroelastic toughening is expected also above the orthorhombic to rhombohedral phase transition temperature.

4.3. Fracture strength

The increase in fracture strength from room temperature to 800 °C cannot be explained by changes in fracture mode, as the fracture mode is transgranular at both temperatures. In addition, the fracture originates from similar defects at both high and low temperature. The observed

diffraction line broadening in machined bars is due to residual machining-induced local strain at the surface. This local strain may reduce the room temperature strength, but strain due to machining is expected to relax at 800 °C. An increase in fracture strength has been measured at room temperature in annealed $La_{1-x}Sr_xFe_{1-y}Co_yO_{3-\delta}$ ceramics (121 ± 7 MPa) relative to as-machined materials (107 ± 15 MPa).[21] Assuming a similar behaviour for $LaFeO_3$ materials, the effect of annealing is within the uncertainty of the current measurements. The increase in fracture strength, σ_f, from room temperature to 800 °C can as a first approximation thus be attributed to the observed increase in fracture toughness, K_{IC}, according to the relation[36]

$$\sigma_f = \frac{K_{IC}}{Y\sqrt{\pi a}} \quad (2)$$

where Y is a dimensionless term determined by the crack configuration and loading geometry and a is half the length of an interior crack or the entire length of an edge crack.

The large porous regions (50–100 μm) in the materials in the present study lower the fracture strength considerably compared to materials with a more homogeneous microstructure. Reducing the flaw size by one order of magnitude would give an increase in the fracture strength by a factor of $\sqrt{10}$, according to Eq. (2). This infers that a fracture strength of 400–500 MPa should be well within reach for microstructurally homogeneous $LaFeO_3$ ceramics.

5. Conclusions

Ferroelastic behaviour of $LaFeO_3$ ceramics is demonstrated by a partial hysteresis loop measured under cyclic compression. The coercive stress is in the order of 20 MPa, and the residual strain after application of a stress of 500 MPa is 0.025%. Ferroelastic toughening was observed, and the variation in fracture toughness with temperature correlates with the magnitude of the crystallographic strain. The maximum fracture toughness observed is 3.1 ± 0.3 MPa $m^{1/2}$, measured at 800 °C. The measured fracture strength increases from 202 ± 18 MPa at room temperature to 235 ± 38 MPa at 800 °C due to the increase in fracture toughness between these temperatures.

The strength and toughness of $LaFeO_3$ both at low and elevated temperatures are high compared to data reported for perovskites with similar and lower porosity. The promising mechanical properties make $LaFeO_3$ a potential candidate as a load-bearing material in high-temperature devices.

Acknowledgements

The authors thank NTNU and the Research Council of Norway for financial support and Knut Olav Helleseng, Per Erik Vullum and Randi Holmestad for performing the TEM investigations.

References

1. Eibschütz, M., Shtrikman, S. and Treves, D., *Phys. Rev.* 1967, **156**, 562–577.
2. Mahadevan, P., Shanthi, N. and Sarma, D. D., *J. Phys. Condens. Mater.* 1997, **9**, 3129–3138.
3. Arakawa, T., Kurachi, H. and Shiokawa, J., *J. Mater. Sci.* 1985, **20**, 1207–1210.
4. Huang, K., Lee, H. Y. and Goodenough, J. B., *J. Electrochem. Soc.* 1998, **145**, 3220–3227.
5. Mizuzaki, J., Sasamoto, T., Cannon, W. R. and Bowen, H. K., *J. Am. Ceram. Soc.* 1982, **65**, 363–368.
6. Mizuzaki, J., Sasamoto, T., Cannon, W. R. and Bowen, H. K., *J. Am. Ceram. Soc.* 1983, **66**, 247–252.
7. ten Elshof, J. E., Bouwmeester, H. J. M. and Verveij, H., *Solid State Ionics* 1995, **81**, 97–109.
8. ten Elshof, J. E., Bouwmeester, H. J. M. and Verweij, H., *Solid State Ionics* 1996, **89**, 81–92.
9. Traversa, E., Matsushima, S., Okada, G., Sadaoka, Y., Sakai, Y. and Watanabe, K., *Sens. Actuat. B: Chem.* 1995, **25**, 661–664.
10. van Hassel, B. A., ten Elshof, J. E. and Bouwmeester, H. J. M., *Appl. Catal. A* 1994, **119**, 279–291.
11. Carotta, M. C., Butturi, M. A., Martinelli, G., Sadaoka, Y., Nunziante, P. and Traversa, E., *Sens. Actuat. B: Chem.* 1997, **44**, 590–594.
12. Atkinson, A., *Solid State Ionics* 1997, **95**, 249–258.
13. Atkinson, A. and Ramos, T. M. G. M., *Solid State Ionics* 2000, **129**, 259–269.
14. Hendriksen, P. V., Larsen, P. H., Mogensen, M., Poulsen, F. W. and Wiik, K., *Catal. Today* 2000, **56**, 283–295.
15. Montross, C. S., Yokokawa, H., Dokia, M. and Bekessy, L., *J. Am. Ceram. Soc.* 1995, **78**, 1869–1872.
16. Paulik, S. W., Baskaran, S. and Armstrong, T. R., *J. Mater. Sci.* 1998, **33**, 2397–2404.
17. Baskaran, S., Lewinsohn, C. A., Chou, Y. S., Qian, M., Stevenson, J. W. and Armstrong, T. R., *J. Mater. Sci.* 1999, **34**, 3913–3922.
18. Drennan, J., Zelizko, V., Hay, D., Ciacchi, F. T., Rajendran, S. and Badwal, S. P. S., *J. Mater. Chem.* 1997, **7**, 79–83.
19. Paulik, S. W., Baskaran, S. and Armstrong, T. R., *J. Mater. Sci. Lett.* 1999, **18**, 819–822.
20. Chou, Y.-S., Stevenson, J. W., Armstrong, T. R. and Pederson, L. R., *J. Am. Ceram. Soc.* 2000, **83**, 1457–1464.
21. Lein, H. L., Einarsrud, M.-A. and Grande T., Department of Materials Technology, NTNU, Trondheim, Norway, unpublished.
22. Orlovskaya, N., Kleveland, K., Grande, T. and Einarsrud, M.-A., *J. Eur. Ceram. Soc.* 2000, **20**, 51–56.
23. Sammes, N. M. and Ratnaraj, R., *J. Mater. Sci.* 1995, **30**, 4523–4526.
24. D'Souza, C. M. and Sammes, N. M., *J. Am. Ceram. Soc.* 2000, **83**, 47–52.
25. Kleveland, K., Orlovskaya, N., Grande, T., Moe, A. M. M., Einarsrud, M.-A., Breder, K. *et al.*, *J. Am. Ceram. Soc.* 2001, **84**, 2029–2033.
26. Aizu, K., *J. Phys. Soc. Jpn.* 1969, **27**, 387–396.
27. Abrahams, S. C., Barns, R. L. and Bernstein, R. L., *Solid State Commun.* 1972, **10**, 379–381.
28. Orlovskaya, N. and Gonzalez, I. N., *J. Mater. Process Manuf.* 2000, **9**, 53–63.
29. Déchamps, M., de Leon Guevara, A. M., Pinsard, L. and Revcolevschi, A., *Phil. Mag. A* 2000, **80**, 119–127.
30. Kim, C. H., Jang, J. W., Cho, S. Y., Kim, I. T. and Hong, K. S., *Physica B* 1999, **262**, 438–443.
31. Fossdal, A., Doctoral thesis, Norwegian University of Science and Technology, Trondheim, Norway, 2003, in press.
32. Geller, S. and Raccah, P. M., *Phys. Rev. B* 1970, **2**, 1167–1172.
33. Geller, S. and Wood, E. A., *Acta Crystallogr.* 1956, **9**, 563–568.
34. Salje, E. K. H., *Phase Transitions in Ferroelastic and Co-elastic Crystals*. Cambridge University Press, Cambridge, 1990.

35. ISO/CD 15732, *Fine ceramics (Advanced ceramics, Advanced Technical Ceramics)—Test Method for Fracture Toughness at Room Temperature by Single Edge Precracked Beam (SEPB) Method*. International Organization for Standardization, Geneva, Switzerland.
36. Richerson, D. W., *Modern Ceramic Engineering*. Marcel Dekker Inc., New York, 1992.
37. Bueble, S., Knorr, K., Brecht, E. and Schmahl, W. W., *Surf. Sci.* 1998, **400**, 345–355.
38. Walsmley, J. C., Bardal, A., Kleveland, K., Einarsrud, M.-A. and Grande, T., *J. Mater. Sci*. 2000, **35**, 4251–4260.
39. Fett, T., Munz, D. and Thun, G., *J. Am. Ceram. Soc*. 1998, **81**, 269.
40. Fett, T., Munz, D. and Thun, G., *J. Eur. Ceram. Soc*. 2003, **23**, 195.
41. Glazounov, E., Kungl, H., Reszat, J.-T. and Hoffmann, M. J., *J. Am. Ceram. Soc.* 2001, **84**, 2921–2929.
42. Faaland, S., Vullum, P. E., Grande, T., Holmestad, R. and Einarsrud, M.-A., unpublished.
43. Müllner, P. and Kriven, W. M., *J. Mater. Res.* 1997, **12**, 1771–1776.
44. Virkar, A. V., Jue, J. F., Smith, P., Mehta, K. and Prettyman, K., *Phase Trans.* 1991, **35**, 27–46.
45. Mehta, K. and Virkar, A. V., *J. Am. Ceram. Soc.* 1990, **73**, 567–574.